ISSN 2232-9080

Received: 13.03.2026.
Reviewed: 27.05.2026.
Accepted: 02.06.2026.

e-ZBORNIK 31/2026

Electronic collection of papers of the
Faculty of Civil Engineering University of Mostar

Original scientific paper
https://doi.org/10.47960/2232-9080.2026.31.16.1

Determination, mapping and analysis of heat islands in the urban area of the City of Mostar using satellite imagery

Josip Alpeza
University of Zagreb, Faculty of Geodesy, B.Sc. (Geod. and Geoinf.), jalpeza@geof.hr
Andrea Marić
University of Zagreb, Faculty of Geodesy, B.Sc. (Geod. and Geoinf.), amaric@geof.hr
Olga Bjelotomić Oršulić
University North, Department of Geodesy and Geomatics, Ph.D., oborsulic@unin.hr
Sanja Šamanović
University North, Department of Geodesy and Geomatics, Ph.D., sasamanovic@unin.hr

Abstract: This paper analyzes the occurrence of urban heat islands in the City of Mostar using satellite imagery from the Landsat mission. Land Surface Temperature (LST) was derived from the thermal band for the summer period from 2021 to 2025. The analysis was conducted in a GIS environment using LST and spectral indices NDVI, NDWI, NDBI and BSI, which enable the identification of vegetated areas, water bodies, built-up surfaces and bare soil. Based on these parameters, the Environmental Criticality Index (ECI) was calculated to assess the level of thermal vulnerability in different parts of the urban area. The results indicate a clear relationship between land cover characteristics and LST and ECI values. Built-up areas and bare soil are associated with higher temperatures, while vegetation and water bodies exhibit a pronounced cooling effect. The obtained results, presented through an interactive web map, provide insight into the spatial distribution of urban heat islands and may serve as a basis for urban planning and increasing the proportion of green areas.

Key words: urban heat islands (UHI), environmental criticality index (ECI), urban green islands, land surface temperature (LST), urban heat island web map, Mostar

Određivanje, kartiranje i analiza toplinskih otoka urbanog područja Grada Mostara primjenom satelitskih snimki

Sažetak: U ovom radu je analizirana pojava urbanih toplinskih otoka (UTO) na području Grada Mostara primjenom satelitskih snimki misije Landsat. Površinska temperatura tla (LST) određena je korištenjem termalnog kanala za ljetno razdoblje od 2021. do 2025. godine. Analiza je provedena u okviru GIS-a primjenom LST-a i spektralnih indeksa NDVI, NDWI, NDBI i BSI koji omogućuju izdvajanje vegetacijskih, vodenih, izgrađenih površina te golog tla. Na osnovi dobivenih parametara izračunat je indeks kritičnosti okoliša (ECI) kojim je procijenjena razina toplinske ugroženosti pojedinih dijelova urbanog prostora. Rezultati ukazuju na jasnu povezanost između karakteristika zemljišnog pokrova te LST-a i ECI-ja. Izgrađene površine i golo tlo povezani su s višim temperaturama, dok vegetacija i vodene površine imaju izražen rashlađujući učinak. Dobiveni rezultati, realizirani u obliku web-karte, omogućuju uvid u prostornu raspodjelu urbanih toplinskih otoka te mogu poslužiti kao podloga za planiranje urbanog razvoja i povećanje udjela zelenih površina.

Ključne riječi: urbani toplinski otoci (UTO), indeks kritičnosti okoliša (ECI), urbani zeleni otoci, površinska temperatura tla (LST), web-karta urbanih toplinskih otoka, Mostar

1. INTRODUCTION

Satellite imagery is an important source of spatial data, as it enables the analysis of changes on the Earth's surface, including the monitoring of urbanization, changes in land cover, and climate conditions [1, 2].

To monitor temperature as an important climatic factor, images captured by thermal sensors are frequently used to measure two types of temperature: air temperature and Land Surface Temperature (LST). Air temperature is normally measured at a height of 2 meters at meteorological stations [3], while LST describes the thermal state of the surface itself and depends heavily on the type of land cover. It is measured at specific heights directly above the ground (5 cm and higher) [4], and is often estimated precisely through the analysis of images acquired by thermal sensors (such as the TIRS on Landsat 8 and 9), which measure the emitted infrared radiation in the thermal part of the spectrum (from 8 to 14 μm). The sensors register the emitted infrared radiation and convert it into surface temperature data, and are capable of detecting very small changes (less than 0.1°C) [1, 5].

In the context of global temperature rise and increasingly intensive urbanization, the phenomenon of Urban Heat Islands (UHI), or the increase in land and air temperatures due to concentrated urbanization, has attracted particular attention. Developing cities and decreasing share of natural surfaces result in an increase in temperature compared to surrounding areas. Systematic monitoring of a specific area using remote sensing provides detailed information on the spatial distribution of surface temperature and temperature behavior depending on the type of land cover. Based on these values, conclusions can be drawn about the presence of heat islands within a city [5, 6].

UHIs represent parts of a city where the surface temperature is higher than that of the surrounding area, with elevated temperatures negatively affecting human health and quality of life. The reason for their formation is the prevalence of artificial materials in the composition of structural elements in the area, namely concrete and asphalt, which heat up differently than natural soils, especially vegetation and water. This results in an increase in the area's temperature by several degrees Celsius compared to the surrounding undeveloped land. Their formation is also influenced by urban density, which can further elevate temperatures [5, 6]. UHIs potentially develop further due to heavy traffic, fossil fuel combustion, and a high proportion of paved surfaces, reflecting the combined effect of temperature and the lack of cooling factors (water and vegetation) in urban environments [7, 8]. To describe the impact of urbanization on the thermal state of the environment, research is often performed using various indicators that correlate surface temperature and land cover characteristics. One of such indicators is the Environmental Criticality Index (ECI), which measures the impact of urbanization on the environment and serves to identify areas exposed to increased environmental pressures due to urbanization, or to assess the level of thermal vulnerability of an area [9, 10].

On the other hand, we can also speak of urban green islands. These are parts of the city where air and soil temperatures are lower than in the surrounding area, primarily thanks to vegetation, which acts as a natural cooling agent by providing shade and water evaporation, thereby mitigating the impact of heat islands [11]. Vegetation absorbs the blue and red parts of the spectrum necessary for photosynthesis and reflects the green and near infrared parts, thus contributing to environmental cooling [12]. The presence of vegetation and the creation of shade in a city are therefore crucial, particularly in the summer months when air temperatures, and especially ground temperatures, are very high [13].

The objective of this paper is to identify, map, and analyze UHIs in the City of Mostar using satellite images from the Landsat mission, and to analyze their relationship with land cover

characteristics and the degree of urbanization. The occurrence of UHIs is the subject of numerous studies. Due to increasing urbanization and climate change, the UHI phenomenon has in recent years been at the center of numerous international studies analyzing the correlation between LST and land cover characteristics [14]. The spatial distribution of LST and its relationship with land cover characteristics can be analyzed using remote sensing and satellite imagery. A study in Türkiye (Kayseri, Cappadocia) established that an increase in the share of built-up areas and a decrease in vegetation lead to an increase in LST and the intensification of UHIs [15]. For the area of Brazil (Sao Paulo), the relationship between LST and spectral indices NDVI and NDBI was analyzed, where it was confirmed that vegetation and water surfaces have a pronounced cooling effect, while built-up areas and bare soil contribute to an increase in temperature [16]. In a similar study conducted for the area of Cyprus (Paphos), UHIs were analyzed using remote sensing, demonstrating that a combined analysis of LST and spectral indices enables the effective identification of thermally stressed urban areas and the assessment of urbanization's impact on the thermal state of the environment [17]. Also, one of the studies emphasizes that satellite imagery and spectral index analysis represent a reliable approach for monitoring the spatial distribution of UHIs and changes in the thermal conditions of urban environments [18]. Similar studies have also been conducted in Croatia and Bosnia and Herzegovina. For instance, in the area of Varaždin, UHI dynamics were analyzed based on LST and spectral index calculations, identifying changes associated with urbanization and the reduction of vegetation cover [19]. Another example is the analysis of UHI distribution in the area of Zagreb using LST and ECI, which identified areas of increased thermal vulnerability in the city center and around industrial plants [10]. Of particular interest is a study conducted for the City of Mostar [20], which analyzed LST distribution over a longer time period, identifying the main areas of elevated temperatures associated with urbanized and industrial surfaces. This study represents an important starting point for identifying UHIs in the Mostar area and serves as a baseline for the further analysis conducted in this paper.

Although UHIs have frequently been investigated using satellite data, research focused on Bosnia and Herzegovina, and especially on the city of Mostar, remains very limited. For the Mostar area, previous studies primarily analyzed long-term changes in LST until 2018, while more recent changes associated with the intensification of urbanization and the increase in air temperature have been insufficiently investigated. Also, integrated analyses that link LST with multiple spectral indices and environmental criticality indicators in the context of urban heat islands are practically non-existent for this area. Therefore, the aim of this paper is to analyze the spatial distribution of UHIs in the Mostar area using satellite imagery from the Landsat 8/9 missions (active Landsat missions with a thermal band) and to assess the level of environmental criticality, or ECI, using LST and spectral indices.

This research was carried out within the project ''The influence of the 3D structure of a city on the intensity of the urban heat island'' (UNIN-TEH-26-1-4), University North, Varazdin, Croatia (2026).

2. PURPOSE OF THE RESEARCH

The area of the City of Mostar was selected to investigate and understand the occurrence and distribution of UHIs. Mostar has distinctly warm climatic characteristics resulting from its location in the Neretva River valley and proximity to the Adriatic Sea. According to the Köppen climate classification, Mostar belongs to the Csa type, or Mediterranean climate with hot and dry summers and mild and wetter winters [21]. It is one of the warmest urban areas in Southeastern Europe. It is precisely here that the highest air temperature of the countries formed by the breakup of the former Yugoslavia was recorded: 46.2°C, measured on 31 July 1901 [21]. This record has not been broken to this day. The mean annual air temperature is 15°C-16°C, while the summer months are characterized by very high temperatures. During heatwaves, daily temperatures can exceed 40°C [21]. Due to these climatic conditions, the area is particularly suitable for studying UHIs. The geographical location of

Mostar further facilitates heat retention. The city is situated in the Neretva valley (below 100 m above sea level) surrounded by mountain massifs (over 500 m above sea level), which can contribute to heat retention, reduced ventilation, and a more difficult inflow of wind that would cool the area. The combination of high summer temperatures, pronounced urbanization, and location in a valley creates favorable conditions for the occurrence and development of UHIs. In addition, land cover types also have a significant impact. Built-up surfaces such as concrete, asphalt, and roofs have a high heat absorption capacity, while vegetation and water areas act as natural temperature regulators. Precisely because of these differences in the thermal properties of various surfaces [22], UHIs in Mostar can be highly pronounced, especially during the summer months.

A study has already been conducted for the area of the City of Mostar [20] in which the LST of Mostar was determined using satellite methods. The study was conducted for the period from 1999 to 2018. However, recent changes associated with urbanization and the increase in air temperatures after 2018 have not been analyzed in detail. Previous research for Mostar focused mainly on LST analysis, without detailed integration of spectral indices or an assessment of the thermal vulnerability of the urban space. Unlike LST itself, which considerably depends on the meteorological conditions present at the time of image acquisition, integrating LST and spectral indices into the ECI enables a more comprehensive assessment of the thermal vulnerability of urban areas. In this way, the analysis is not based solely on the current thermal state of the surface, but also on land cover characteristics that also influence the development of UHIs. Additionally, this paper covers the recent period from 2021 to 2025, which was not included in previous studies for the Mostar area. On a global scale, a significant and continuous rise in air temperatures is currently taking place, with projections indicating further growth until at least 2050 [23]. Furthermore, numerous media reports confirmed in the last year, 2025, that Mostar is the warmest city in Southeastern Europe [24, 25]. Due to the obvious trend of temperature increase and dense development, the City of Mostar, as such, represents a suitable area for the formation of UHIs, where urbanization results in high thermal vulnerability.

This paper analyzes UHIs in the Mostar area for the period 2021–2025 by combining LST with spectral indices that represent key land cover types relevant to the thermal behavior of urban space. Based on the integrated analysis, the spatial identification of UHIs and the assessment of thermal vulnerability of urban space can be conducted. One of the contributions of this study is in the operationalization of the results through a publicly accessible interactive web map, which enables spatial and temporal UHI analysis and can serve as a tool for spatial planning and climate adaptation of urban space.

The objective of the research is to identify the areas of the city where urbanization significantly contributes to the increase in LST, thereby leading to severe environmental criticality. Based on the data, conclusions are drawn regarding the distribution of urban heat islands, and the final step is to map these areas. It is assumed that the highest LST values are associated with areas of the highest urbanization and a lower proportion of vegetation and water surfaces.

3. ANALYSIS AREA

The area of the City of Mostar is located in Bosnia and Herzegovina, in the central part of the Herzegovina-Neretva County, and covers an area of 1,166.12 km². It consists of 60 settlements [26].

For the purpose of conducting the research, the settlement of Mostar and its suburban settlements were selected based on two criteria. The first criterion is the level of development of the area. The analysis included settlements with a higher proportion of built-up areas, with additional consideration of the spatial proximity to the settlement of Mostar. The proportion of built-up areas was assessed by visual interpretation of satellite images (Landsat 8 images for the period 2021–2025, ESRI World Imagery [27], and Google Maps [28]) as well as cartographic bases (OpenStreetMap [29]),

where residential, industrial, and traffic zones were classified as built-up areas. The second criterion is the population size (more than 1,000 inhabitants) according to the 2013 population census in Bosnia and Herzegovina [30]. The urban and suburban areas of Mostar where urbanization is expected to have a more pronounced effect on the formation of UHIs were identified in this way.

A total of 21 settlements of the City of Mostar are included: Mostar, Ilići, Cim, Rodoč, Vihovići, Gnojnice, Raštani, Vrapčići, Potoci, Kutilivač, Vojno, Buna, Blagaj, Lakševine, Ortiješ, Kosor, Dračevice, Jasenica, Bačevići, Hodbina, and Željuša. The study area covers a total of 194 km². The selected settlements encompass the urban and suburban areas with a higher proportion of built-up surfaces, while the remaining 39 settlements have a predominantly rural character with dominant vegetation cover and are therefore not included in the analysis of urban heat islands. A view of the selected area within the City of Mostar is presented in Figure 1.

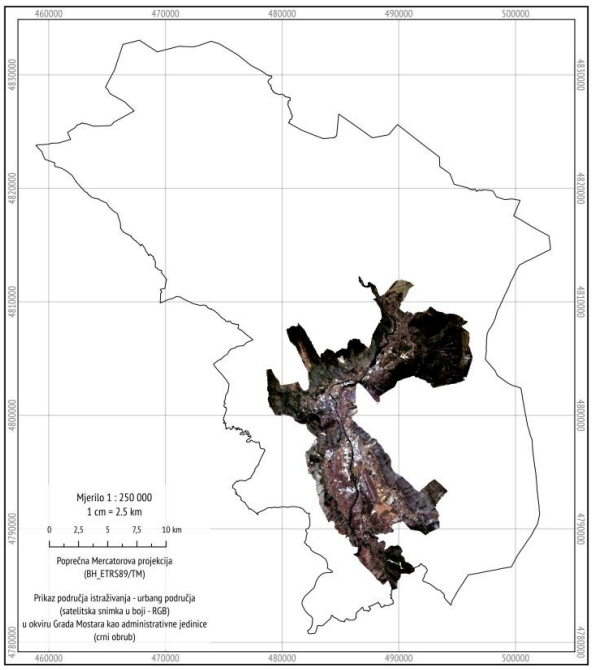

Figure 1. View of the study area within the administrative boundaries of the City of Mostar with the analyzed area marked

4. RESEARCH METHODOLOGY

The methodology of the study is based on processing satellite images to calculate LST and identify areas with pronounced heat islands in the City of Mostar. The distribution of UHIs was determined using the ECI, which provides insight into different levels of vulnerability of a specific area due to heat retention.

All satellite image processing and analysis were carried out using the GIS tool QGIS (version 3.32, "Lima"), and the results are presented in the form of LST and ECI web maps. The web map was created using the "QGIS2WEB" plugin, partially edited via Visual Studio Code, and then published on the GitHub platform.

4.1 Data sources

To determine and map UHIs in the City of Mostar area, satellite images serve as the primary source of data. Images from the Landsat 8 mission, acquired from the US Geological Survey (USGS) via the Earth Explorer interface [31], were used for processing. This is the only free mission that offers the higher-resolution thermal images required for this study (for instance, Sentinel lacks thermal bands, while MODIS provides kilometer-resolution images). The spatial resolution of the multispectral images (bands 1–7 and 9) is 30 m, the panchromatic band (band 8) has a spatial resolution of 15 m, while the thermal images (bands 10 and 11) have a spatial resolution of 100 m [32]. The thermal bands (10 and 11) used in this study have a spatial resolution of 100 m and for the purpose of the analysis they were resampled to 30 m to match the resolution of the multispectral bands. Band 10 will be used for LST and UHI analysis, given that band 11 has certain calibration issues, although it also acquires data in the thermal part of the spectrum [33].

The summer period, from 1 June to 31 August, was considered for the images acquired from 2021 to 2025. One cloud-free image (0% cloud cover) was acquired for each year. This helps avoid unreliable results, since cloud cover can create a false impression of the conditions in an area over which it is present. Clouds are generally cooler than the surface areas beneath them; consequently, the resulting image pixels will exhibit lower LST values.

Five Level-1 images acquired on 13 August 2021, 15 July 2022, 11 July 2023, 18 June 2024, and 8 August 2025 were downloaded. All images were acquired by the Landsat 8 satellite between 11:27 and 11:34 local time (UTC+2, CEST). Since a single cloud-free satellite image was used for each year, the results represent the state of LST and thermal vulnerability at the time of image acquisition and do not reflect the full seasonal dynamics. Meteorological conditions at the time of image acquisition, such as short-term temperature variations, air humidity, or prior precipitation, may influence the representativeness of the results.

The second data source used consists of administrative units, namely the City of Mostar, its city districts, and settlements. For the purposes of this paper, these were provided by the City of Mostar, Department of Urban Planning and Construction, Cadastral Service [26]. It contains geometric and attribute data for the City of Mostar and its settlements in ESRI Shapefile format.

4.2 Selection of cartographic projection

The original satellite images are available in the Universal Transverse Mercator projection (UTM, zone 33). The images were reprojected into the official coordinate system of the Federation of Bosnia and Herzegovina, BH_ETRS89/TM (EPSG: 10329), which is a new cartographic projection of the Federation of Bosnia and Herzegovina based on ETRS89. The second data source used, administrative boundaries, is still available in the old Gauss–Krüger projection (DKS1901), which remains widely used in practice. The reason for this is the gradual transition of official spatial data to the new reference system [34].

The use of the new BH_ETRS89/TM projection in this study also contributes to the gradual transition to the new reference system and may encourage its wider use in future research and papers.

4.3 Land cover classification

Conducting the analysis and drawing conclusions about areas with UHIs requires an initial land cover classification.

The classes were determined using a supervised, or semi-automated classification method. The classes used in this study were defined by selecting representative pixels from the images to serve as

training samples for individual classes to perform the classification. Based on these defined samples, the satellite imagery classification was performed using the Minimum Distance method, which assigns pixels to each class based on the training sample by following their normal (Gaussian) distribution, where the distance from the distribution mean serves as a measure of similarity between an individual pixel and the representative class sample [35].

A detailed visual inspection indicated the presence of four land cover macro-classes within the study area, each comprising specific classes: water (with Neretva River and lakes as classes), vegetation (with trees, forests, and grasslands as classes), bare soil (arable land and rocky terrain), and built-up land (roads, houses, and buildings). These macro-classes were chosen due to their dominant presence in the Mostar area, as well as their distinct thermal properties and influence on LST and ECI. Other land cover classes (e.g., burned areas) were not observed, while unclear parts of the images were excluded from the classification process. The selection of the four land cover macro-classes is based on the research objective and the spatial resolution of the Landsat 8 multispectral images used (30 m). At this level of spatial resolution, it is not possible to reliably distinguish more detailed urban sub-classes, such as high- and low-rise buildings, because a single pixel often covers several different surfaces. A more detailed analysis of urban elements, such as building density, building height, or other material types (other than roof surfaces of houses and buildings), would require higher spatial resolution imagery and additional data on buildings.

Classification was performed for each of the selected datasets from the five-year period using the blue, green, red, and near-infrared Landsat 8 bands (bands B2–B5). Representative samples of individual classes were identified through visual interpretation of the satellite images themselves, as well as the ESRI World Imagery [27] and Google Maps [28] satellite basemaps. The selection of these macro-classes and their internal classes is based on their dominant presence within the urban area of the City of Mostar and their influence on LST and the occurrence of UHIs. The quality of the classification was assessed by comparing the classified values of each raster with reference points identified by visual interpretation of RGB composite satellite images, with the resulting overall classification accuracy presented in Table 1.

The classification accuracy assessment was conducted at the level of land cover macro-classes. This approach was adopted because each class belongs to one of the macro-classes (e.g., the arable land class falls under bare soil), and any classification errors at the individual class level are reflected in the overall accuracy of the corresponding macro-class and, consequently, in the overall classification accuracy. Approximately one hundred reference points were identified for each macro-class, for which visual inspection enabled reliable assignment to one of the four macro-classes, while avoiding mixed pixels. To avoid defining reference points for all five images separately, efforts were made to identify points corresponding to the same locations across all images. Considering the objective of the study, which focuses on analyzing the spatial distribution of UHIs, as well as the limited spatial resolution of the Landsat 8 imagery (30 m), the validation at the macro-class level and the results shown in Table 1 can be considered satisfactory. The poorest classification result was obtained for the year 2023, while the highest classification accuracy was achieved for the 2024 image.

Table 1. Overall classification accuracy by image

Image (Year)	Overall classification accuracy
2021	82%
2022	88%
2023	77%
2024	91%
2025	85%

The spatial resolution of the Landsat 8 multispectral bands (30 m) and thermal bands (100 m) used in this study represents a limitation of the research, particularly in urban areas where mixed pixels may occur within a single pixel due to varying land cover. Consequently, individual pixels may contain a mixture of built-up surfaces, vegetation, and bare soil, which can affect the accuracy of both the classification and LST determination.

4.4 Surface emissivity values

All values within the macro-classes were reclassified using emissivity values of different objects. Emissivity is the ratio of thermal energy radiated by an object to that of an ideal black body, and is defined by the expression [36]:

$$e_\lambda = \frac{M_{\lambda\,(\text{object, T})}}{M_{\,(\text{black body, T})}} \tag{1}$$

Emissivity values vary depending on the type of land cover and play a significant role in determining LST [37]. In this study, mean emissivity values for individual land cover macro-classes were adopted from the literature [38]. Based on the performed classification, each macro-class was assigned a corresponding emissivity value, which was used in the subsequent LST calculation process.

The obtained emissivity values used in this study are presented in Table 2. They represent mean values for each individual macro-class.

Table 2. Emissivity values for individual macro-classes [38]

Macro-class	Emissivity value
Water	0.980
Built-up area	0.937
Vegetation	0.982
Bare soil	0.928

4.5 Calculation of land surface temperature (LST)

Raw data recorded in the form of digital numbers (DN) need to be converted into a format suitable for further processing and the calculation of LST and ECI. Thermal band 10 is therefore converted into top-of-atmosphere spectral radiance, then into top-of-atmosphere reflectance, followed by the retrieval of brightness temperature [39], after which LST can be calculated. The thermal infrared band is particularly useful for estimating LST and studying UHIs. Band 10 was used here, with a central (effective) wavelength of λ = 10.895 μm. Band 11 was disregarded due to the previously mentioned calibration issues. All calculations were carried out using QGIS, specifically its "Raster Calculator" tool.

LST in degrees Celsius (originally expressed in Kelvin, requiring conversion of the temperature scale, where 0 K = −273.15 °C) is obtained using the following expression [39]:

$$\text{LST [°C]} = \frac{T_B}{1 + \frac{\lambda \cdot T_B}{C_2} \cdot \ln(\varepsilon)} - 273.15 \tag{2}$$

where C_2 is the second radiation constant, based on the expression [40]:

$$C_2 = h\frac{c}{k} \tag{3}$$

where h is Planck's constant, equal to $6.626 \cdot 10^{-34}$ J s, and c is the speed of light, $c = 2.998 \cdot 10^8$ m/s. The value k is Boltzmann's constant, $k = 1.381 \cdot 10^{-23}$ J/K. Substituting these constants yields $C_2 = 1.4388 \cdot 10^{-2}$ mK. Since wavelengths expressed in micrometers are often used in Equation (2), the second radiation constant is therefore 14388 μmK. The T_B value represents the brightness temperature, or the satellite-derived radiance temperature in Kelvin, which is calculated using the following formula [39]:

$$T_B = \frac{K_2}{\ln\left(\frac{K_1}{L_\lambda} + 1\right)} \tag{4}$$

where K_1 and K_2 are thermal conversion constants related to the band defined in the metadata file of each image. In this case, for thermal band 10, $K_1 = 774.8853$ and $K_2 = 1321.0789$. Equation (4) also uses L_λ, which represents top-of-atmosphere (TOA) spectral radiance, obtained as follows [39]:

$$L_\lambda = M_L Q_{cal} + A_L \tag{5}$$

where M_L is the band-specific multiplicative scaling factor from the metadata file (for band 10 it is 0.00033), Q_{cal} is the quantized standard pixel value, i.e., the image digital number, and A_L is the band-specific additive scaling factor from the metadata file (for band 10 it is 0.1).

In this way, LST values were obtained for all five images, and an additional view of the mean summer land surface temperature for the period 2021–2025 was created.

4.6 Calculation of the Environmental Criticality Index (ECI)

The ECI, which is used as an indicator of urban thermal vulnerability, can be calculated from LST and spectral indices. In the literature, the basic form of the ECI is defined as a simple ratio of LST to NDVI [41]:

$$ECI = \frac{LST}{NDVI} \tag{6}$$

However, this formula does not account for multiple surface types; it only considers vegetation while ignoring water bodies and, in particular, built-up areas, which are actually key to defining UHIs. Therefore, an extended expression from the literature [41], which includes water bodies and built-up land, was used:

$$ECI = \frac{LST + NDBI}{NDVI + NDWI} \tag{7}$$

where NDVI is the Normalized Difference Vegetation Index, defined as the ratio of the difference to the sum of the near-infrared and red parts of the spectrum [42]; NDBI is the Normalized Difference Built-Up Index, represented as the ratio of the difference to the sum of the shortwave-infrared and near-infrared part of the spectrum [43]; and NDWI is the Normalized Difference Water Index, defined as the ratio of the difference to the sum of the green and near-infrared parts of the spectrum [44]. They are calculated according to the following expressions:

$$NDVI = \frac{NIR - RED}{NIR + RED} \quad (8)$$

$$NDBI = \frac{SWIR - NIR}{SWIR + NIR} \quad (9)$$

$$NDWI = \frac{GREEN - NIR}{GREEN + NIR} \quad (10)$$

In this way, Equation (7) incorporates the main land cover types: water and vegetation, which reduce the heat island effect, and built-up areas, which cause temperature increases and consequently UHI formation due to their material composition.

Bare soil was also included on a test basis to explore the possibility of extending the ECI so as to encompass all macro-classes, since bare soil is currently the only macro-class not included in the ECI calculation. The Bare Soil Index (BSI) was introduced and calculated according to the following expression [45]:

$$BSI = \frac{(SWIR + RED) - (NIR + BLUE)}{(SWIR + RED) + (NIR + BLUE)} \quad (11)$$

and Equation (7) was extended under the assumption that ECI (and LST) are directly proportional to BSI: as BSI increases (indicating the presence of bare soil, such as rocky areas and arable land), ECI (and LST) also increases, and vice versa:

$$ECI = \frac{LST + NDBI + BSI}{NDVI + NDWI} \quad (12)$$

ECI was calculated for two scenarios: without BSI and with BSI, i.e., according to Equation (7) and Equation (12), respectively. The use of BSI is purely experimental and represents an addition to Equation (12).

Urbanized areas, as the primary cause of UHIs, are identified by the spectral index NDBI, which measures the intensity of development (surfaces such as concrete, asphalt, and roofs). On the other hand, water surfaces exert a strong cooling effect on the environment, particularly due to evaporation. Without NDWI, the model does not distinguish between vegetation and water surfaces, although they have different thermal effects. NDVI provides a clear indication of vegetation density and health, as well as the ability of vegetation to cool the surface through the evaporation of water from plant leaves [42, 43, 44]. Combining LST with NDBI already provides an indication of the warmer parts of the city characterized by higher land surface temperatures (particularly due to the development level and density) while relating them with NDVI and NDWI yields a stronger contrast between hotter and cooler parts of the city. The selected spectral indices represent the main land cover types that influence LST and are commonly used in UHI studies to analyze the relationship between land cover and LST [46]. This study also examined the relationship between LST and the spectral indices used. The linear relationship between the variables was assessed using Pearson's correlation coefficient (r), whose values range from −1 (perfect negative correlation, where two variables are inversely proportional) to 1 (perfect positive correlation, where the variables are directly proportional) [47]:

$$r = \frac{\sum(x_i - \bar{x})(y_i - \bar{y})}{\sqrt{\sum(x_i - \bar{x})^2} \cdot \sqrt{\sum(y_i - \bar{y})^2}} \quad (13)$$

where x represents the LST values, y represents the spectral index values, and $\bar{x}$ and $\bar{y}$ are their respective mean values. The expression can be simplified by using the covariance of the variables and their standard deviations [47]:

$$r = \frac{cov(X,Y)}{\sigma_x \sigma_y} \quad (14)$$

For the purposes of calculating Equations (7) and (12), the spectral indices NDBI, NDVI, NDWI, BSI and LST itself were reclassified. Mean values of the indices and LST for the period 2021-2025 were used. The values were reclassified from the values [-1, 1] for the indices, and [0, 50] for LST, to the values [0, 1]. As a result, ECI values will also range from 0 to 1. Reclassifying the indices and LST to the same measurement scale ensures a balanced contribution of each parameter in the final ECI value and avoids the dominance of one factor over the others.

The numerical values of the ECI [0, 1] need to be converted into understandable environmental criticality levels, i.e. the values need to be quantified. Water surfaces are included in the ECI calculation using NDWI since the presence of water significantly reduces the thermal vulnerability of an area. However, water surfaces themselves are not included in the classification of environmental criticality levels because they do not represent areas susceptible to the development of UHIs. Therefore, they are separated by the NDWI mask and shown as a separate category.

ECI categories are divided into classes of equal intervals, as presented in Table 3. Since only summer Landsat 8 images were used in the study, ECI is interpreted in the context of summer thermal vulnerability of urban areas and the occurrence of UHIs. ECI values would therefore need to be adjusted into classes for winter, for example, since thermal vulnerability is not present during that period, or is not expressed to the same extent as during the summer months.

Table 3. Environmental criticality (thermal vulnerability) classes

Class	Environmental criticality level
0.00–0.10	no environmental criticality
0.11–0.21	very low environmental criticality
0.22–0.32	low environmental criticality
0.33–0.44	moderately low environmental criticality
0.45–0.55	moderate environmental criticality
0.56–0.66	moderately high environmental criticality
0.67–0.77	high environmental criticality
0.78–0.88	very high environmental criticality
0.89–1.00	severe environmental criticality

4.7 Mapping of urban heat islands and green islands

The development of a web map of LST for the period 2021–2025 and of thermal vulnerability, or ECI, represents a way of visualizing the research results and aims to present the spatial distribution of heat and green islands in the City of Mostar. The map is designed as an interactive display that provides users with a clear and well-laid-out insight into the differences in the area's thermal vulnerability depending on the built-up areas, the amount of vegetation and the distribution of water surfaces.

The map is enriched with attribute data that provide information on the temperature value for LST, or on the environmental criticality (thermal vulnerability) for ECI. The rasters are vectorized (polygonized) so as to preserve their attributes. The interactive web map was created and exported from QGIS using the ''QGIS2WEB'' plugin [48], which enables local web-based viewing of the map on the user's computer.

The web map generated by ''QGIS2WEB'' has somewhat weaker cartographic design and contains numerous redundant details, so the generated HTML document was edited and reduced (from 7000, mostly redundant, lines of code to 600). The display was designed using the Leaflet [49] library, a free and open JavaScript library for creating interactive web maps. A well-designed cartographic display was achieved by editing the CSS, with the aim of improving the map appearance and user interface, and the JavaScript, to enable map interactivity. The code was edited using Visual Studio Code [50], a free, feature-rich code editor developed by Microsoft.

Two displays were designed separately. The first is the "Map of Summer Land Surface Temperatures," showing summer temperatures for summer days from 2021 to 2025, as well as the mean summer temperature for the same period, using two basemaps: a satellite image (ESRI World Imagery, a basemap of high-resolution satellite and aerial imagery ranging from 30 cm to 1 m, according to specifications for urban areas [27], which provides a detailed representation of the Earth's surface) and a cartographic basemap (set as the primary and simple basemap, the Voyager layer [51], similar to OpenStreetMap but with slightly improved style and faster loading speed). Both basemaps were provided with an option to increase or decrease visibility for easier map navigation. The second display is the "Map of Heat and Green Islands," designed in the same way as the first map; however, it primarily presents environmental criticality levels, that is, thermal vulnerability within the City of Mostar.

Both maps allow filtering—by temperature in the first display and by criticality levels in the second—for a clearer view and better insight into map elements, as well as the temperature and environmental criticality scales, and include the option to display the user's location. Additionally, the summer temperature map enables a chronological display of temperatures, automatically switching between layers to visually track LST changes over time within a specific area. The map is enhanced by adding a coordinate grid displaying locations in WGS84 (geodetic latitude ϕ and longitude λ), the old Gauss-Krüger projection (y and x values), and the new Transverse Mercator projection BH_ETRS89/TM (E and N values).

The two separate cartographic displays were integrated into one through the design of an entry portal, enabling users to perceive them as a single unit and access them through a single web interface. Additionally, the web map was adapted for viewing on mobile devices.

For global display, to enable all users to open the web map, it has been hosted on a global server, GitHub [52], which is a free and popular platform for storing and sharing program code, as well as for hosting web maps. The web map was stored as a repository with all accompanying files, and a link was subsequently generated on the entry portal enabling access to the web map.

Finally, the web map was indexed, or added to Google's database via Google Search Console, enabling users to access it through a search engine by entering keywords (e.g. "Mostar heat island map") and thus not depending solely on the direct link to the published map.

5. RESULTS

The results include the spatial distribution of LST and ECI in the City of Mostar and an analysis of the relationship between LST, ECI and land cover spectral indices.

5.1 Land surface temperature

LST exhibits significant spatial differences in the study area during the observed period. The lowest values were registered in the mountainous area of the Kutilivač settlement, near the Veliko Pločno peak (1440 m a.s.l.). In all analyzed images, the minimum temperatures were recorded in that area: about 21°C on 13 August 2021 and 15 July 2022, about 20°C on 11 July 2023, 18°C on 18 June 2024, and about 15°C on 8 August 2025.

The highest land surface temperatures were recorded in highly urbanized and industrial areas, as well as on large open asphalted surfaces. Thus, on 13 August 2021, a temperature of 46°C was recorded in the Aluminij industrial complex located in the settlement of Bačevići. In the image from 15 July 2022, the highest values, about 47°C, were recorded in the area of Mostar Airport and, once again, in the Aluminij industrial zone. During 2023, maximum temperatures were somewhat lower, with approximately 41°C recorded on 11 July in the area of the military barracks in the settlement of Rodoč. In the image from 18 June 2024, the highest temperature of approximately 43 °C was recorded in the area of the Soko industrial complex, while on 8 August 2025 the highest value (42 °C) was again recorded in the airport area.

The mean summer land surface temperature for the period 2021–2025 shows a similar spatial distribution. The lowest mean temperatures were recorded in the mountainous area of Kutilivač (about 19°C). The Neretva River watercourse is slightly warmer than that area. The highest temperature values were recorded in the southern part of the urban area, particularly in the airport and industrial zones, where mean temperatures reach 41°C to 43°C. The mean temperature for the entire Mostar area is 32°C.

Only the area of the settlement of Mostar was separated and analyzed using the mean LST layer. A mean temperature of 33°C was recorded. The minimum temperature of 28°C was recorded along Neretva and north of Zalik, and the maximum temperature of almost 39°C was recorded in Bišće Polje.

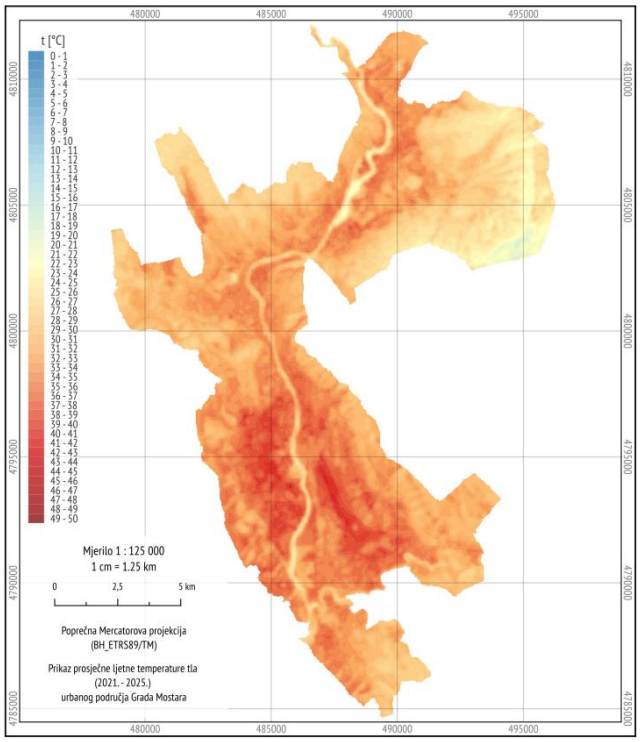

Figure 2. Mean summer land surface temperature in the area of the City of Mostar (2021–2025)

Mean summer land surface temperatures in the Mostar area are presented in the map shown in Figure 2, while a comprehensive overview of temperatures for all analyzed dates (2021–2025), together with the mean temperature, can be viewed on the developed web map of summer temperatures [53].

5.2 Environmental criticality

ECI was calculated from the averaged LST values (Figure 2) and from the indices shown in Figure 3, namely NDVI (a), NDWI (b), NDBI (c), and BSI (d). Higher positive values (up to a maximum of 1) of each index are shown in a darker grey color and indicate the presence of vegetation for NDVI, water for NDWI, built-up areas for NDBI, and bare soil for BSI. NDVI has the highest values in areas with dense vegetation cover, especially in mountainous and rural parts of the study area. NDWI clearly highlights the water surfaces of the Neretva River. On the other hand, NDBI shows higher values in urbanized parts of the city, industrial zones and the airport area. Higher values of BSI are observed in areas of bare soil and rocky surfaces.

The calculation of ECI according to Equations (7) and (12) resulted in very similar index values. For this reason, the mapped ECI obtained according to Equation (7), which is also used in the literature [41], is also presented.

The distribution of thermal vulnerability classes of individual areas of the City can be observed by visual inspection alone. Thus, serious environmental criticality was observed in certain parts of the Mostar settlement, especially in the industrial zone and around the airport. These areas are called urban heat islands. They are also surrounded by areas with slightly lower, but still high, criticality: very high, high and moderately high environmental criticality. The UHIs are located primarily along the Neretva River, and overlap with the built-up areas of the City. South of Bišće Polje, the heat islands spread westward and eastward, extending into the areas of the settlements of Rodoč, Jasenica,

Gnojnice, Bačevići, Dračevice and Blagaj. They were also observed in industrial zones, at the Uborak landfill, in the Gajevi business zone, at the Zinktehnik plant, east of the railway bridge in Raštani, in the area of the Northern Camp, in the industrial area around Bišće Polje and the Southern Camp, at Soko in Rodoč, at the plant near the company Hercegovinavino and the county prison, at Aluminij in Bačevići, and at Mostar Airport. Urban, built-up areas of the settlement of Mostar are also in the "red" zone: Centar, Centar 2 and Centar 3, part of Rudnik, Zgoni, Bijeli Brijeg near the University Clinical Hospital Mostar, Carina, the Mostar railway station, Majdan, Cernica, and part of the Old Town near the Old Bridge. Areas without environmental criticality, i.e. green islands where no thermal vulnerability is present, are also identified. These are the mountainous areas of Vihovići towards Goranci and the peaks of Vrapčići and Kutilivač. In the south, they include parts of Hodbina and Blagaj, as well as Rodoč, Jasenica and Buna. The area of Ilići and Cim is particularly interesting because it is almost entirely in the ''green'' zone, i.e. there is almost no environmental criticality, despite its close connection to the urban area of Mostar and its pronounced suburban characteristics. The settlement area of Mostar was once again specifically examined. Here, urban green islands play a crucial role in counteracting the effects of heat islands and in providing protection against thermal vulnerability. The larger green areas include those towards Miljkovići, Trimuša and the Bare promenade, the southern area of Bijeli Brijeg, and the northern part of Zalik. Most parks and stadiums in the city, such as Zrinjevac and the stadium under Bijeli Brijeg, have low environmental criticality.

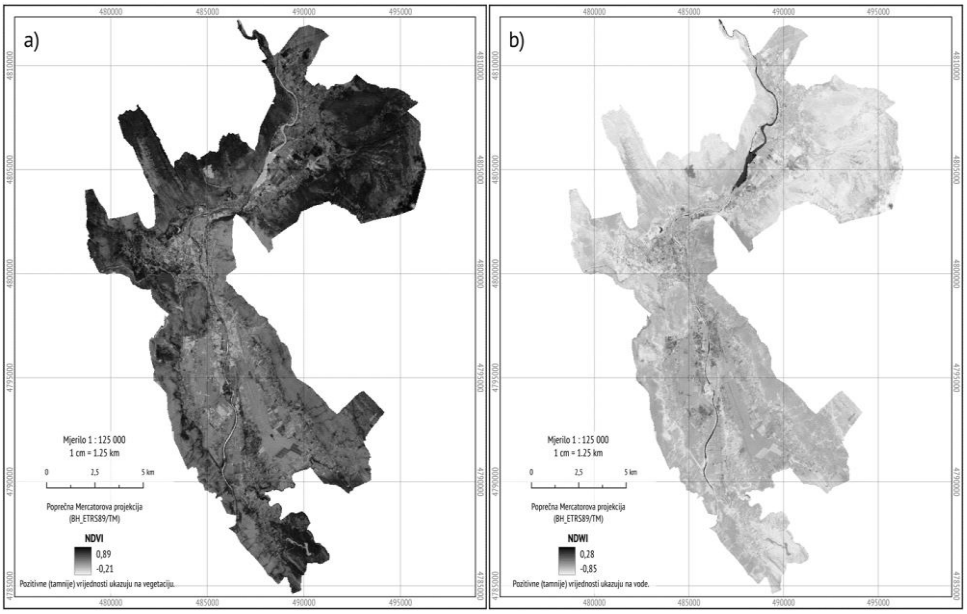

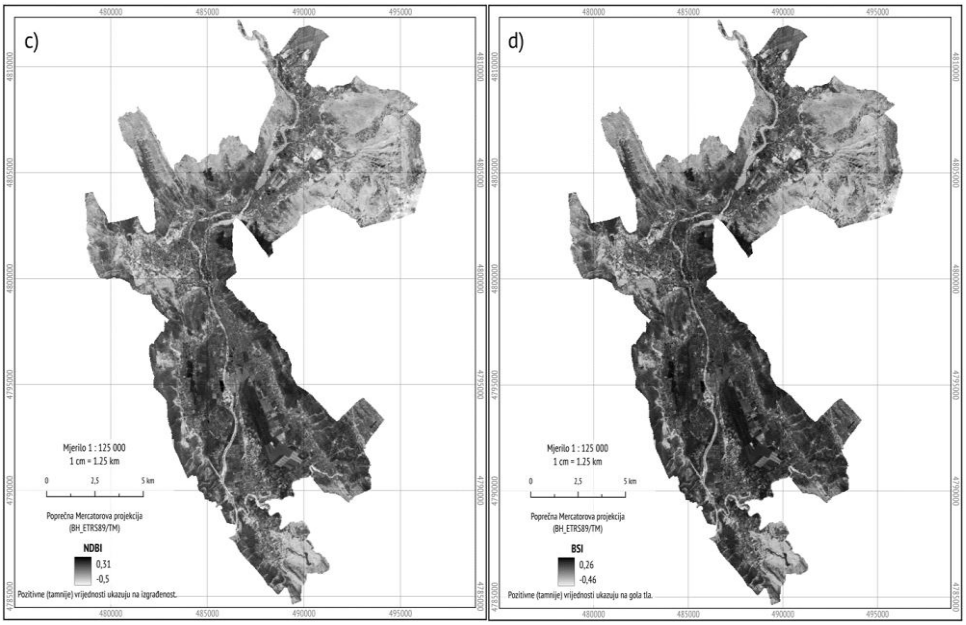

Figure 3. Mean spectral indices: a) NDVI, b) NDWI, c) NDBI and d) BSI

The environmental criticality of the urban part of the City of Mostar, that is, thermal vulnerability in the area of the City of Mostar, is presented in Figure 4. The entire presentation can also be viewed on the web map [53].

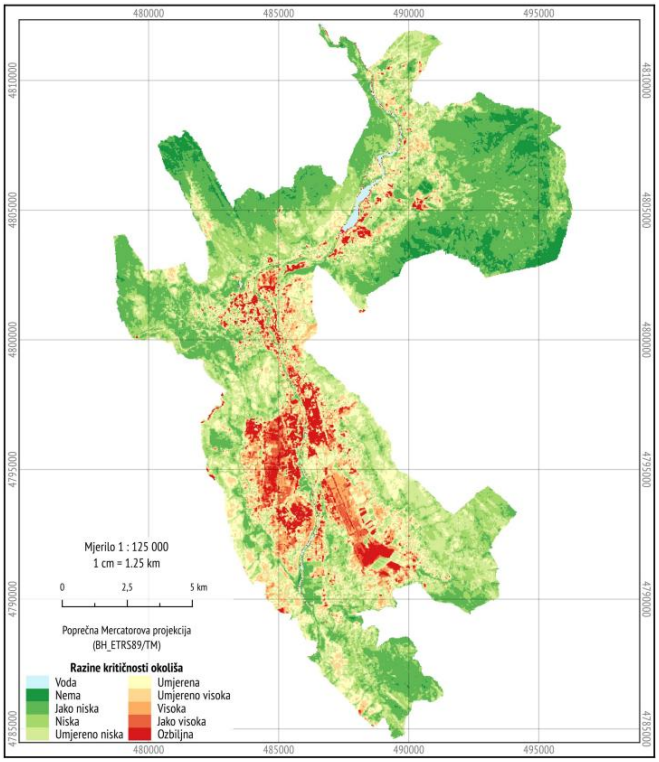

Figure 4. Environmental criticality in the area of the City of Mostar (2021–2025)

5.3 Analysis of results

Since the calculation of ECI directly depends on the parameters included in Equation (7), and LST depends on the land cover classification and reclassification into emissivity values, an evaluation of the UHI identification performance was also conducted. Table 4 shows the mean land surface temperatures by land cover macro-classes: water, vegetation, bare soil and built-up areas, as well as the average environmental vulnerability class.

Table 4. Mean LST and ECI by land cover macro-class

Macro-class	LST [°C]	ECI [environmental criticality]
Water	26.94	None
Vegetation	28.87	Very low
Bare soil	32.85	Moderately low
Built-up areas	35.48	Moderately high

The obtained results show the expected results by land cover macro-classes. Built-up and bare surfaces are characterized by higher LST and ECI values, while vegetation and water surfaces show lower LST and ECI values. The only possible error is associated with water bodies, since they were excluded from the ECI calculation; however, it is evident that some pixels were not removed. Nevertheless, since there is no environmental criticality, it is concluded that the water areas are also successfully classified.

Another analysis was conducted to determine the relationship between LST and land cover macro-classes represented by spectral indices. As presented in Equation (7), it was assumed that an increase in NDBI (higher built-up intensity) leads to a rise in LST (higher temperature), whereas an increase in NDVI (more vegetation) and NDWI (presence of water bodies) results in a decrease in LST (lower temperature). ECI was not tested, since it represents a derived value from the parameters used.

For the purposes of the correlation analysis, the original LST and spectral index rasters were converted into a point dataset, with the corresponding raster value extracted from each pixel. In this way, a dataset of approximately 215,000 observations was obtained, on the basis of which the Pearson correlation coefficient between LST and the individual indices was calculated.

LST data and NDVI, NDWI, NDBI, and BSI data were used independently, yielding the following results: r(LST, NDVI) = –0.66, r(LST, NDWI) = –0.63, r(LST, NDBI) = 0.72, and r(LST, BSI) = 0.73.

The analysis shows that the parameters used are meaningfully related to LST and ECI and consequently that Equations (7) and (12) are well formulated and that LST indeed depends on land cover classes, i.e. that there is a strong correlation between LST and built-up areas, vegetation and water bodies.

The area around the Neretva River was additionally analyzed by creating gradational areas, in order to observe whether water acts as a cooling factor on the surrounding area. The analysis was conducted because there are certain (non-scientific) claims that Neretva is the coldest river in the world [54]. Zones of 5, 10, 20, 50, 100, 200, 500 and 1000 meters from the Neretva River were created, as presented in Table 5.

Table 5. Influence of the Neretva River on thermal vulnerability reduction

Distance [m]	LST [°C]	ECI [environmental criticality]
5	28.46	Very low
10	28.42	Very low
20	28.49	Very low
50	28.66	Very low
100	29.26	Low
200	30.85	Low
500	33.18	Moderately low
1000	34.05	Moderate

The analysis shows that with increasing distance from the Neretva River, the mean LST and ECI values increase. This trend indicates a correlation between the proximity of water surfaces and lower land surface temperatures and lower thermal vulnerability, although the cooling effect of the river cannot be clearly separated from other factors, such as the pronounced urbanization along the river itself and land cover. A marked increase in mean LST values is observed beyond approximately 200 m, which may suggest a diminishing influence of the river on the surrounding area.

Mean LST and ECI values were also analyzed for the settlements of the City of Mostar included in the analysis. Higher values of LST and ECI were recorded in settlements with more pronounced urbanization, industrial areas and a lower proportion of vegetation, such as Bačevići, Kosor, Jasenica, Rodoč and Gnojnice. On the other hand, lower values were recorded in peripheral and more vegetation-rich settlements such as Kutilivač, Potoci, Vihovići, Ilići, and Vrapčići. Such results may be useful when identifying areas for increasing green spaces and for planning measures to mitigate the UHI effect. However, the results should be interpreted with a degree of caution, as they represent averaged values at the settlement level. Consequently, even within settlements with lower mean values, there may be local areas with higher LST and ECI values associated with built-up surfaces, while a higher proportion of vegetation reduces the mean values at the level of the entire settlement. A detailed overview is given in Table 6.

Table 6. Mean LST and ECI by settlements of the City of Mostar

Settlement	LST [°C]	ECI [environmental criticality]
Bačevići	36.12	Moderately high
Kosor	36.11	Moderate
Jasenica	35.89	Moderately low
Rodoč	35.76	Moderate
Gnojnice	35.29	Moderate
Lakševine	35.22	Moderately low
Ortiješ	35.05	Moderately low
Blagaj	34.11	Moderately low
Dračevice	33.74	Moderately low
Buna	33.68	Low
Mostar	33.35	Moderate
Željuša	33.24	Moderately low

Cim	33.12	Low
Hodbina	32.23	Low
Raštani	31.49	Low
Vojno	31.12	Very low
Vrapčići	31.01	Low
Ilići	30.91	Low
Vihovići	30.82	Low
Potoci	29.76	Low
Kutilivač	27.57	None

6. DISCUSSION

The research results clearly show that the spatial distribution of LST and UHIs in the City of Mostar is largely associated with land cover type and the degree of urbanization. The highest temperatures were recorded in areas with a high proportion of built-up surfaces, while the lowest temperatures were present in areas with vegetation cover and near water bodies.

Particularly significant UHIs were observed in areas of industrial and transport infrastructure. The most critical locations were identified in the area of Mostar Airport, the Aluminij industrial zone in Bačevići, the Soko industrial complex in Rodoč, the Bišće Polje industrial area, and the Uborak landfill. At these locations, the highest LST values were recorded, exceeding 40°C in some cases, while ECI values reached the highest thermal vulnerability classes.

The obtained results confirm a strong relationship between LST and land cover characteristics. Correlation analysis showed a positive correlation between LST and NDBI ($r = 0.72$), which confirms that increased urbanization, i.e. built-up areas and materials such as concrete and asphalt, lead to higher surface temperatures. In contrast, a negative correlation was found between LST and NDVI ($r = -0.66$), as well as between LST and NDWI ($r = -0.63$). These results confirm the cooling effect of vegetation and water bodies, due to water evaporation from water surfaces and water in plant leaves, as well as shading provided by vegetation. LST has the strongest correlation with bare soil, or BSI ($r = 0.73$), which indicates that they are strongly related and interdependent. However, this value is almost identical to the correlation between LST and NDBI, indicating that NDBI may to some extent already include certain surface types (e.g., rocky terrain) that exhibit spectral behavior similar to built-up areas. Both indices already include the shortwave-infrared and near-infrared part of the spectrum (with the exception that BSI also incorporates the red and blue bands); therefore, it can be concluded that, since the inclusion of BSI did not lead to significant changes in the distribution of thermally vulnerable areas, it is sufficient to use the built-up index NDBI in Equation (7), as also stated in the literature [41].

A particularly interesting result of the study concerns the influence of the Neretva River on reducing thermal vulnerability in the surrounding area. The analysis of distance from the river course showed a gradual increase in land surface temperature with increasing distance from the river. It is precisely around the Neretva River that built-up density is highest; therefore, higher thermal vulnerability is expected in this area. However, Neretva is clearly a strong factor that significantly reduces LST, as well as the environmental criticality of the areas along the river. This trend confirms the importance of water bodies as a natural regulator of thermal vulnerability in the urban area of the City of Mostar.

The study results also indicate the importance of urban green areas in reducing thermal vulnerability. Areas with a higher proportion of vegetation, such as parks, sports fields, and green zones, show significantly lower LST values. This confirms the importance of planning and preserving urban green areas for the purpose of mitigating the effects of UHIs. Besides, increasing the proportion

of urban green areas and preserving water bodies may represent one of the key measures for reducing thermal vulnerability in urban environments.

The study also has certain limitations. The spatial resolution of 30 meters may limit the accuracy of temperature determination, especially in smaller built-up or green areas. This can be clearly demonstrated using the example of the Neretva River. Since the Neretva River is narrower than 30 m in certain sections, while the spatial resolution of Landsat 8 imagery is also 30 m, and because water occupies only a small portion of some pixels whereas the surrounding land occupies the larger part, mixed pixels are produced. As a result, the area of the Neretva River cannot be accurately represented. Mixed pixels are also created on other surfaces and land cover classes.

Furthermore, the analysis was conducted on a limited number of cloud-free satellite images during the summer period from 2021 to 2025, so the results represent mean values for a relatively short five-year period. The obtained LST values reflect the conditions at the time of image acquisition. LST, and consequently thermal vulnerability, also depend on the meteorological conditions at the time of image acquisition, such as air temperature, soil moisture, precipitation, and atmospheric conditions [55, 56, 57]. Therefore, differences in LST between individual years cannot be fully or definitively attributed solely to urbanization and other spatial changes, but are also partly influenced by prevailing meteorological conditions. For this reason, the analysis focused primarily on the spatial distribution of land surface temperature and thermal vulnerability within the urban area of Mostar, while comparisons between individual years have limited interpretive significance.

Besides, image acquisition was conducted in the late morning, around 11:30, while the hottest part of the day occurs later, approximately between 13:00 and 17:00, so the surfaces have not yet reached their maximum daily heating. In the future, this could change thanks to the planned Copernicus Land Surface Temperature Monitoring (LSTM) mission, which from 2028 is expected to observe the Earth in the same manner as Landsat 8 and 9 satellites, providing primarily temperature data, but with twice the spatial resolution of Landsat (50 m instead of 100 m), higher temporal resolution (2 days instead of 8), and more diverse overpass times [58].

Despite the stated limitations, the study results provide valuable insight into the spatial distribution of UHIs in the area of Mostar. The obtained results are largely consistent with previous studies conducted across the entire area of Mostar. In the study by Duplančić Leder and Leder [20], the distribution of LST for the period from 1999 to 2018 was analyzed and similar areas of increased temperatures were identified, particularly in urbanized and industrial areas of the city. As in this study, the highest temperatures were recorded in areas with a high proportion of built-up areas and sparse vegetation cover, while lower temperatures were observed in areas with vegetation and near water bodies. The consistency between the results of both studies further confirms the reliability of the applied methodology and indicates the stability of the spatial distribution of UHIs in Mostar over a longer period of time.

7. CONCLUSION

Within the study, LST and ECI were calculated and analyzed for the City of Mostar using Landsat 8 satellite imagery for the period 2021–2025, with the aim of identifying heat islands and assessing the thermal vulnerability of the urban area. The integration of LST, and the spectral indices NDVI, NDWI, and NDBI, along with the experimental inclusion of BSI, in the ECI, enabled the spatial identification of areas of increased thermal vulnerability and the analysis of their relationship with land cover characteristics.

The results of the study showed that the highest LST and ECI values occur in built-up and industrial areas, i.e., areas with more intensive urbanization, whereas lower temperatures were observed in

areas with vegetation cover and in the vicinity of water bodies, indicating the significant influence of land cover type on the occurrence of UHIs. The highest LST and ECI values were recorded in the southern and industrial parts of the urban area of Mostar, particularly in the Bišće Polje district and in the settlements of Gnojnice (especially in the vicinity of Mostar Airport), Rodoč, and Bačevići. The lowest values were found in vegetation-rich and higher-elevation areas such as Kutilivač, Potoci, and Vihovići. The mean LST values by land cover macro-classes confirm this relationship: water 26.94 °C, vegetation 28.87 °C, bare soil 32.85 °C, and built-up area 35.48 °C. Correlation analysis confirmed a strong relationship between land cover characteristics and LST, and consequently with ECI. The positive correlation between LST and NDBI (r = 0.72), as well as between LST and BSI (r = 0.73), indicates that built-up surfaces and bare soil contribute to increased temperatures. The negative correlation between LST and NDVI (r = –0.66), as well as between LST and NDWI (r = –0.63), suggests that vegetation and water surfaces act as mitigating, or cooling, factors of thermal conditions.

The obtained results are comparable to those of previous studies conducted in the Mostar area, particularly with regard to the occurrence of elevated LST values in the urban and industrial parts of the city. However, this study extends previous research by including the recent period 2021–2025 and by conducting an integrated analysis of UHIs through the application of the ECI. Unlike the analysis of LST alone, the ECI enables a more comprehensive assessment of thermal vulnerability by integrating LST with land cover characteristics derived from spectral indices. This enabled a clearer spatial identification of areas with increased thermal vulnerability compared to areas richer in vegetation and water bodies, which exhibit lower LST and ECI values. An additional contribution of this study is in the operationalization of the results through a publicly available interactive UHI web map, which provides insight as well as spatial and temporal analysis of thermal vulnerability in the urban area, along with an overview of LST values during the study period.

It can be concluded that the use of satellite imagery is an effective method for determining the spatial distribution of UHIs. The proposed approach can serve as a basis for future UHI research and as support for spatial planning, increasing the proportion of green areas, and climate adaptation of urban areas, with the aim of mitigating the negative effects of UHIs and enhancing the quality of life of the population.

REFERENCES

1. Campbell, J. B., Wynne, R. H.: Introduction to Remote Sensing, Fifth Edition, The Guilford Press, New York, 2011.
2. Kurt, E.: Prikupljanje i obrada prostornih podataka u GIS-u za potrebe uspostave i održavanja jedinstvene evidencije i registra prostornih jedinica, Geodetski glasnik, 2012., no. 42, pp. 44-52
3. Valiente, J. A., Niclos, R., Barbera, M. J., Estrela, M. J.: Analysis of Differences Between Air-land Surface to Estimate Land Surface Air Temperature from MSG Data, EUMETSAT Meteorological Satellite Conference, 2010.
4. https://www.fhmzbih.gov.ba/latinica/AGRO/tempTla.php (22. 02. 2026)
5. Voogt, J. A., Oke, T. R.: Thermal Remote Sensing of Urban Climates, Remote Sensing of Environment, 2003, Vol. 86, Issue 3, pp. 370-384. https://doi.org/10.1016/S0034-4257(03)00079-8
6. Weng, Q.: Thermal Infrared Remote Sensing for Urban Climate and Environmental Studies: Methods, Applications, and Trends, ISPRS Journal of Photogrammetry and Remote Sensing, 2009, Vol. 64, Issue 4, pp. 335–344. https://doi.org/10.1016/j.isprsjprs.2009.03.007
7. Split-Dalmatia County: Climate change mitigation, climate change adaptation and ozone layer protection program of the Split-Dalmatia County, Split, 2023.

8. Santamouris, M.: Analyzing the heat island magnitude and characteristics in one hundred Asian and Australian cities and regions, Science of the Total Environment, 2015, Vol. 512-513, pp. 582-598. https://doi.org/10.1016/j.scitotenv.2015.01.060
9. Jayasinghe, C. B., Withanage, N. C., Mishra, P. K., Abdelrahman, K., Fnais, M. S.: Evaluating Urban Heat Islands Dynamics and Environmental Criticality in a Growing City of a Tropical Country Using Remote-Sensing Indices: The Example of Matara City, Sri Lanka. Sustainability, 2024, Vol. 16, No. 23. https://doi.org/10.3390/su162310635
10. Čmrlec, K.: Određivanje i kartiranje toplinskih otoka u Gradu Zagrebu pomoću satelitskih podataka [Determination and mapping of heat islands in the City of Zagreb using satellite data], graduation thesis, Faculty of Geodesy, University of Zagreb, Zagreb, 2019.
11. Duplančić Leder, T., Bačić, S.: Utjecaj lokalnih klimatskih zona na termalna obilježja grada Splita, Proceedings of the 14th Symposium of Certified Geodetic Engineers - Women in Geodesy, Croatian Chamber of Certified Geodetic Engineers, 2021, pp. 73-80.
12. https://www.earthdata.nasa.gov/learn/tutorials/use-remote-sensing-data-study-vegetation-dynamics (25. 05. 2026)
13. Bowler, D. E., Buyung-Ali, L., Knight, T. M., Pullin, A. S.: Urban greening to cool towns and cities: A systematic review of the empirical evidence, Landscape and Urban Planning, 2010, Vol. 97, pp. 147-155. https://doi.org/10.1016/j.landurbplan.2010.05.006
14. Cheval, S., Amihăesei, V.-A., Chitu, Z., Dumitrescu, A., Falcescu, V., Irașoc, A., Micu, D. M., Mihulet, E., Ontel, I., Paraschiv, M.-G., Tudose, N. C.: A systematic review of urban heat island and heat waves research (1991–2022), Climate Risk Management, 2024, Vol. 44, Art. 100603. https://doi.org/10.1016/j.crm.2024.100603
15. Cetin, M., Ozenen Kavlak, M., Senyel Kurkcuoglu, M. A., Ozturk, G. B., Cabuk, S. N., Cabuk, A.: Determination of land surface temperature and urban heat island effects with remote sensing capabilities: the case of Kayseri, Türkiye, Nat Hazards, 2024, Vol. 120, pp. 5509-5536. https://doi.org/10.1007/s11069-024-06431-5
16. Venkatraman, S., Kandasamy, V., Rajalakshmi, J., Sabarunisha Begum, S., Sujatha, M.: Assessment of urban heat island using remote sensing and geospatial application: A case study in Sao Paulo city, Brazil, South America, Journal of South American Earth Sciences, 2024, Vol. 134, Art. 104763. https://doi.org/10.1016/j.jsames.2023.104763
17. Dimitriou, Ch., Michaelides, S., Themistocleous, K., Hadjimitsis, D. G., Papadavid, G., Gitas, I., Kyriakides, N.: Assessing the Urban Heat Island (UHI) Effect Using Land Surface Temperature (LST) and Normalized Difference Built-Up Index (NDBI): A Case Study on Paphos, Cyprus, Environmental and Earth Sciences Proceedings, 2025, Vol. 35, No. 1, Art. 65. https://doi.org/10.3390/eesp2025035065
18. Kimothi, S., Thapliyal, A., Gehlot, A., Aledaily, A. N., Gupta, A., Bilandi, N., Singh, R., Malik, P. K., Akram, S. V.: Spatio-temporal fluctuations analysis of land surface temperature (LST) using remote sensing data (LANDSAT TM5/8) and multifractal technique to characterize the urban heat islands (UHIs), Sustainable Energy Technologies and Assessments, 2023, Vol. 55, Art. 102956. https://doi.org/10.1016/j.seta.2022.102956
19. Šamanović, S., Bjelotomić Oršulić, O., Krajina, T., Markovinović, D.: Tracking Urban Heat Island Dynamics Using Open Source Tools and Free Data, The International Archives of the Photogrammetry, Remote Sensing and Spatial Information Sciences, 2025, Vol. 48, pp. 217-224. https://doi.org/10.5194/isprs-archives-XLVIII-4-W13-2025-217-2025
20. Duplančić Leder, T., Leder, N.: Mostar area land surface temperature determination with satellite methods, Collection of Papers of the Faculty of Civil Engineering, University of Mostar, Faculty of Civil Engineering, Architecture and Geodesy, No. 15, 2018, pp. 66-75.
21. https://www.fhmzbih.gov.ba/latinica/KLIMA/klimaBIH.php (22. 02. 2026)

22. Soltanifard, H., Amani-Beni, M.: The cooling effect of urban green spaces as nature-based solutions for mitigating urban heat: insights from a decade-long systematic review, Climate Risk Management, 2025, Vol. 49, Art. 100731. https://doi.org/10.1016/j.crm.2025.100731
23. Wang, L., Wang, L., Li, Y., Wang, J.: A century-long analysis of global warming and Earth temperature using a random walk with drift approach, Decision Analytics Journal, 2023, Vol. 7, Art. 100237. https://doi.org/10.1016/j.dajour.2023.100237
24. https://www.jutarnji.hr/vijesti/svijet/u-mostaru-pao-temperaturni-rekord-za-2025-u-ovom-dijelu-europe-15600322 (24. 02. 2026)
25. https://apnews.com/article/western-balkan-drought-heatwave-no-rainfall-2843b95842e75807a608e7eaa57a96f1 (24. 02. 2026)
26. https://www.mostar.ba/odjel-za-urbanizam-i-gradenje/ (25. 02. 2026)
27. https://www.arcgis.com/home/item.html?id=10df2279f9684e4a9f6a7f08febac2a (03. 03. 2026)
28. https://www.google.com/maps (25. 05. 2026)
29. https://www.openstreetmap.org/ (25. 05. 2026)
30. https://fzs.ba/index.php/category/popis-2013/ (25. 02. 2026)
31. https://earthexplorer.usgs.gov/ (27. 02. 2026)
32. https://www.usgs.gov/landsat-missions/landsat-8 (27. 02. 2026)
33. https://www.usgs.gov/landsat-missions/landsat-8-oli-and-tirs-calibration-notices (25. 05. 2026)
34. Federal Administration for Geodetic and Real Property Affairs. (2019). *Rulebook on Basic Geodetic Works* (Official Gazette of the Federation of Bosnia and Herzegovina, No. 15/19). Sarajevo, https://www.fgu.com.ba/en/
35. Wacker, A. G., Landgrebe, D. A.: Minimum Distance Classification in Remote Sensing, Laboratory for Applications of Remote Sensing, Indiana, 1972. https://doi.org/10.1016/j.rse.2012.12.008
36. Li Z.-L., Tang, B.-H., Wu, H., Ren, H., Yan, G., Wan, Zh., Trigo, I. F., Sobrino, J. A.: Satellite-derived land surface temperature: Current status and perspectives, Remote Sensing of Environment, 2013, Vol. 131, pp. 14-37.,
37. Yu, X., Guo, X., Wu, Z.: Land Surface Temperature Retrieval from Landsat 8 TIRS-Comparison between Radiative Transfer Equation-Based Method, Split Window Algorithm and Single Channel Method, Remote Sensing, 2014, Vol. 6, No. 10, pp. 9829-9852. https://doi.org/10.3390/rs6109829
38. Bustamante, M., Mora, D., Austin, M. C.: Use of Land Surface Temperature Estimation with Geographical Information Tools for Validation of Numerical Microclimate Studies at Urban Scale, E3S Web of Conferences, 2021, 76th Italian National Congress, Vol. 312, Art. 06004. https://doi.org/10.1051/e3sconf/202131206004
39. https://www.usgs.gov/media/files/landsat-8-data-users-handbook (28. 02. 2026)
40. Tran, M.: Planck's and Callendar's Blackbody Radiation Formulas and Their Fitness to Experimental Data, City University of New York, New York, 2019.
41. Češić, M., Rogulj, K., Krtalić, A.: Combined Thermal Index Development for Urban Heat Island Detection in Area of Split, Croatia, Land, 2025, Vol. 14, No. 1, Art. 175. https://doi.org/10.3390/land14010175
42. Lillesand, Th. M., Kiefer, R. W., Chipman, J. W.: Remote Sensing and Image Interpretation, 7th Edition, John Wiley & Sons, New York, 2015.
43. Zha, Y., Gao, J., Ni, S.: Use of normalized difference built-up index in automatically mapping urban areas from TM imagery, International Journal of Remote Sensing, 2003, Vol. 24, No. 3, pp. 583-594. https://doi.org/10.1080/01431160304987
44. McFeeters, S. K.: The use of the normalized difference water index (NDWI) in the delineation of open water features, International Journal of Remote Sensing, 1996, Vol. 17, No. 7, pp. 1425-1432. https://doi.org/10.1080/01431169608948714

45. Rikimaru, A., Roy, P. S., Miyatake, S.: Tropical forest cover density mapping, Tropical Ecology, 2002, No. 43, pp. 39-47
46. Guha, S., Govil, H., Gill, N., Dey, A.: Analytical study on the relationship between land surface temperature and land use/land cover indices, Annals of GIS, 2020, No. 26, pp. 201–216. https://doi.org/10.1080/19475683.2020.1754291
47. Walpole, R. E., Myers, R. H., Myers, S. L., Ye, K.: Probability and Statistics for Engineers and Scientists, 9th Edition, Pearson Education, 2016.
48. https://qgis.org/ (03. 03. 2026)
49. https://leafletjs.com (03. 03. 2026)
50. https://vscode.dev/?vscode-lang=hr-hr (03. 03. 2026)
51. https://carto.com/blog/new-voyager-basemap (03. 03. 2026)
52. https://github.com/ (03. 03. 2026)
53. https://web-karta.github.io/karta-toplinskih-otoka-mostar/ (03. 03. 2026)
54. https://www.worldatlas.com/articles/which-is-the-coldest-river-in-the-world.html (03. 03. 2026)
55. Zhou, D., Zhao, Sh., Liu, Sh., Zhang, L., Zhu, Ch.: Surface urban heat island in China's 32 major cities: Spatial patterns and drivers, Remote Sensing of Environment, 2014, Vol. 152, pp. 51-61. https://doi.org/10.1016/j.rse.2014.05.017
56. Naserikia, M., Hart, M. A., Nazarian, N., Bechtel, B., Lipson, M., Nice, K. A.: Land surface and air temperature dynamics: The role of urban form and seasonality, Science of The Total Environment, 2023, Vol. 905, Art. 167306. https://doi.org/10.1016/j.scitotenv.2023.167306
57. Hong, T., Heo, Y.: Exploring the impact of urban factors on land surface temperature and outdoor air temperature: A case study in Seoul, Korea, Building and Environment, 2023, Vol. 243, Art. 110645. https://doi.org/10.1016/j.buildenv.2023.110645
58. https://sentiwiki.copernicus.eu/web/lstm (03. 03. 2026)